Electronic Supplementary Material (ESI) for Soft Matter.
This journal is © The Royal Society of Chemistry 2019

Electronic Supplementary Information

1. Analytic solution of indentation of a rigid sphere into an elastic substrate with surface tension and adhesion

By Hui et al.[1], an analytic solution for the indentation problem of a rigid sphere into an elastic substrate with surface stress and adhesion is given as

$$F_0^{\mathrm{Hui}} = \frac{16\mu}{3R}\left(\frac{a}{\hat{a}}\right)^3 \hat{P}, \tag{S1}$$

where $\hat{a}$ and $\hat{P}$ can be solved implicitly by

$$\begin{aligned} 0 &= 3\bar{\delta}_H(\beta)\hat{a}^2 - 4\phi(\beta)\sqrt{\frac{\hat{a}}{\Lambda(\beta)}} \\ \hat{P} &= -\bar{P}_H(\beta)\hat{a}^3 + 2\sqrt{\frac{\hat{a}^3}{\Lambda(\beta)}} \end{aligned}, \tag{S2}$$

and

$$\begin{aligned} &\beta = \frac{\sigma}{2\mu a}, \quad \phi(\beta) = \frac{0.6425\beta^2 + 4.284\beta + 1.0}{0.2039\beta^3 + 3.994\beta^2 + 6.011\beta + 1.0}, \quad \Lambda(\beta) = \frac{2.0\beta^2 + 7.4\beta + 1.0}{\pi\beta^3 + 15.78\beta^2 + 10.92\beta + 1.0}, \\ &\bar{\delta}_H(\beta) = 1 + \frac{1}{3}\ln\left(1 + 6.582\beta + 2.759\beta^2 + 0.3782\beta^3\right), \quad \bar{P}_H(\beta) = 1 + \frac{3\pi\beta}{4}\frac{\beta^2 + 0.6016\beta + 0.0171}{\beta^2 + 0.3705\beta + 0.0063}. \end{aligned} \tag{S3}$$

2. Bulk elasticity and surface stress contribution with large sphere radius (*R*=21.7 microns)

To justify our statement in section 3.3, a similar simulation is done with a larger sphere *R*=21.7 microns. As shown in Fig. S1, the elastic contribution is still small compared to surface stress contribution at *D*=0, while indeed increases a bit compared to *R*=11.8 microns case.

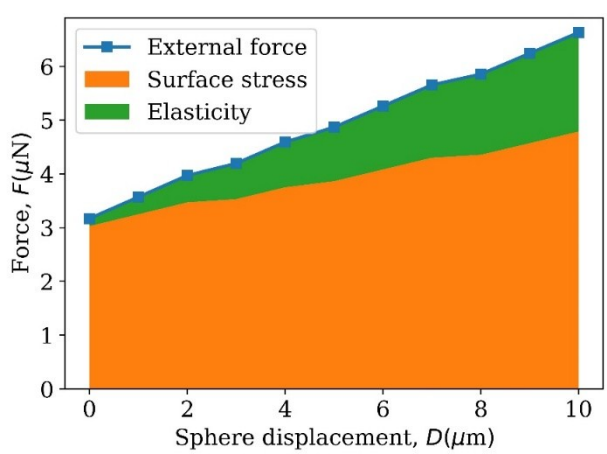

Fig. S1. Contribution to the total external force from surface stress (orange stacked area) and from elasticity (green stacked area) versus sphere displacement, using a 21.7-μm-radius sphere. Ratio of the contributions from bulk elasticity to surface stress increases as the sphere displacement increases.

3. Force versus displacement for different FE models.

Here we compare the FE results of external force F versus the sphere displacement D for sphere radius R=17.4 microns case. As shown in Fig. S2, the FE model 2 (bi-material and bi-surface stress model) underestimates the external force severely, comparing to the FE model 1 we have used throughout this work. In the beginning, the external force predicted by FE model 2 is only about 70% of model 1; as the displacement increases, the external force by FE model 2 starts to drop down while the FE model 1 still correctly captures the magnitude of external force and the linear relationship between the force and displacement before instability occur, which is consistent with experiments[2].

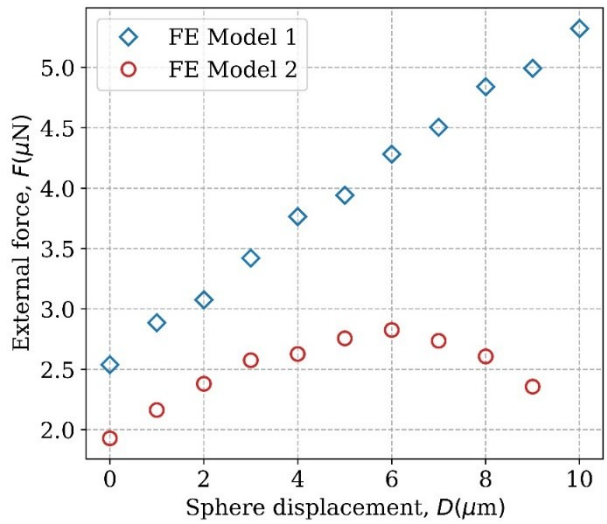

Fig. S2. External force F plotted versus sphere displacement D for different FE models. Results of FE model 1 and model 2 are plotted as blue and red symbols, respective.

4 Anisotropic surface stress model: theory and FE implementation

Consider a curve in the r-z plane of an axisymmetric surface (Fig.2 in the main text). The *unit* tangent, binormal, and normal vectors are denoted by $\mathbf{t}(s), \mathbf{b}(s)$ and $\mathbf{n}(s)$, respectively. The surface deformation gradient then is

$$\mathbf{F}_s = \lambda_1^s \mathbf{t} \otimes \mathbf{t} + \lambda_2^s \mathbf{b} \otimes \mathbf{b} \tag{S4}$$

where λ_1^s and λ_2^s are the surface stretches in the principal directions $\mathbf{t}$ and $\mathbf{b}$, respectively. Define the right surface Cauchy-Green tensor as $\mathbf{C}_s = \mathbf{F}_s^{\mathrm{T}} \mathbf{F}_s$. The surface free energy is assumed to takes the following form:

$$W = W\left(I_1^s, J_s\right) = A\left(I_1^s - 2\right) + \sigma_0\left(J_s - 1\right) + \frac{1}{2} B\left(J_s - 1\right)^2 \tag{S5}$$

where $I_1^s = \mathrm{tr}\left(\mathbf{C}_s\right)$ and $J_s = \det\left(\mathbf{F}_s\right)$. Hence the surface stress tensor $\boldsymbol{\sigma}_s$ is anisotropic and given by[3–5]

$$\boldsymbol{\sigma}_s = \frac{2A}{J_s} \mathbf{F}_s \mathbf{F}_s^{\mathrm{T}} + \left[\sigma_0 + B\left(J_s - 1\right)\right] \mathbf{1} \,. \tag{S6}$$

Note $\boldsymbol{\sigma}_s = \sigma_{tt} \mathbf{t} \otimes \mathbf{t} + \sigma_{bb} \mathbf{b} \otimes \mathbf{b}$ in the basis of $\{\mathbf{t}, \mathbf{b}\}$ (i.e., no shear component), each component can be expressed explicitly as,

$$\sigma_{tt} = 2A\frac{\lambda_1^s}{\lambda_2^s} + \sigma_0 + B\left(\lambda_1^s\lambda_2^s - 1\right)$$
$$\sigma_{bb} = 2A\frac{\lambda_2^s}{\lambda_1^s} + \sigma_0 + B\left(\lambda_1^s\lambda_2^s - 1\right) \tag{S7}$$

To find out the equilibrium equations, we parametrize the axisymmetric surface $\mathbf{r}$ by the in-plane (*r*-*z* plane) curve's arclength, *s*, and the rotation angle about the z-axis, θ, by

$$\mathbf{r} = \mathbf{r}(s,\theta) = \left(f(s)\cos\theta, f(s)\sin\theta, g(s)\right), \quad f(s) \neq 0 \tag{S8}$$

from an open set

$$U = \left\{(s,\theta) \in \mathbf{R}^2; -\infty < s < \infty, 0 \le \theta < 2\pi\right\}. \tag{S9}$$

Hence, the tangent vectors (not unit) are

$$\mathbf{g}_1 = \frac{\partial \mathbf{r}}{\partial s} = \left(f'\cos\theta, f'\sin\theta, g'\right)$$
$$\mathbf{g}_2 = \frac{\partial \mathbf{r}}{\partial \theta} = \left(-f\sin\theta, f\cos\theta, 0\right) \tag{S10}$$

and the corresponding Christoffel symbols given by Do Carmo[6] are

$$\Gamma_{11}^1 = \frac{f'f'' + g'g''}{(f')^2 + (g')^2} = 0, \quad \Gamma_{22}^1 = -\frac{ff'}{(f')^2 + (g')^2} = -ff'$$
$$\Gamma_{12}^2 = \Gamma_{21}^2 = \frac{f'}{f}, \quad \Gamma_{22}^2 = \Gamma_{11}^2 = \Gamma_{21}^1 = \Gamma_{12}^1 = 0 \tag{S11}$$

where we have used $(f')^2 + (g')^2 = 1$ and $f'f'' + g'g'' = 0$.

In the basis of $\{\mathbf{g}_1, \mathbf{g}_2\}$, $\boldsymbol{\sigma}_s = \sigma^{\alpha\beta}\mathbf{g}_\alpha \otimes \mathbf{g}_\beta$, $\alpha, \beta = 1, 2$. Note $\boldsymbol{\sigma}_s$ dependents on *s* only and has no shear components. The equilibrium equations yield[3–5]

$$\sigma^{\alpha\beta}b_{\alpha\beta} + [\sigma]^{33} = 0, \quad \sigma^{\alpha\beta}{}_{|\alpha} + [\sigma]^{\beta 3} = 0 \tag{S12}$$

where $[\boldsymbol{\sigma}]$ represents the discontinuity of the true Cauchy stress across the interface in the deformed configuration, and $[\sigma]^{33}$, $[\sigma]^{\beta 3}$ are the normal and shear components of $[\boldsymbol{\sigma}]\cdot\mathbf{n}$. The stroke stands for the covariant differentiation. The first equation of (S12) stands for the Laplace pressure balanced by the jump of normal stress of the bulk; the second one stands for the Marangoni stress resisted by the jump of shear stress of the bulk. For the second equation of (S12) in the direction of $\mathbf{g}_1$ ($\beta = 1$),

$$\sigma^{\alpha 1}{}_{|\alpha} = \sigma^{11}{}_{|1} + \sigma^{21}{}_{|2} \tag{S13}$$

and,

$$\sigma^{11}{}_{|1} = \frac{\partial \sigma^{11}}{\partial s} + \Gamma_{\gamma 1}^1\sigma^{\gamma 1} + \Gamma_{\gamma 1}^1\sigma^{1\gamma} = \sigma^{11}{}_{,1} + \Gamma_{11}^1\sigma^{11} + \Gamma_{21}^1\sigma^{21} + \Gamma_{11}^1\sigma^{11} + \Gamma_{21}^1\sigma^{12} = \sigma^{11}{}_{,1} \tag{S14}$$

$$\sigma^{21}{}_{|2} = \frac{\partial \sigma^{21}}{\partial \theta} + \Gamma_{\gamma 2}^1\sigma^{\gamma 2} + \Gamma_{\gamma 2}^2\sigma^{1\gamma} = 0 + \Gamma_{12}^1\sigma^{12} + \Gamma_{22}^1\sigma^{22} + \Gamma_{12}^2\sigma^{11} + \Gamma_{22}^2\sigma^{12} = \Gamma_{22}^1\sigma^{22} + \Gamma_{12}^2\sigma^{11} \tag{S15}$$

Combining (S11) and (S13)-(S15) yields

$$\sigma^{11}{}_{,1} - f f' \sigma^{22} + \frac{f'}{f}\sigma^{11} = -[\sigma]^{13} \tag{S17}$$

Notice that $\mathbf{g}_1 = \mathbf{t}$ and $\mathbf{g}_2 = f\mathbf{b}$, we have $\sigma^{11} = \sigma_{tt}$ and $\sigma^{22} = \frac{1}{f^2}\sigma_{bb}$, and then (S17) can be rewritten as

$$\frac{\partial \sigma_{tt}}{\partial s} - \frac{f'}{f}\sigma_{bb} + \frac{f'}{f}\sigma_{tt} = -[\sigma]^{13} \tag{S18}$$

which is identical to Style and Xu[7].

For the second equation in the direction $\mathbf{g}_2$ ($\beta = 2$), it can be easily checked that the equilibrium equation is satisfied by noticing $[\sigma]^{23}$ is trivial due to axi-symmetry.

To quantitatively simulate this anisotropic surface behaviors, we implemented a new 2-node surface finite element for nonlinear, implicit, static, axisymmetric finite element simulations. The surface moduli in these calculations are chosen so that when the surface is subjected to an equiaxial state of stress, the surface mechanical behaviors are consistent with the isotropic surface model. Specifically, in (S7), we enforce $2A + \sigma_0 = 20$ mN/m and $2A + B = 120$ mN/m to match the initial surface stress and hardening behaviors. When $A = 0$, it collapses to the case of isotropic surface stress, which is our FE model 1 in the main text. We also study another extreme case: $A = 10$ mN/m, $\sigma_0 = 0$ and $B = 100$ mN/m. The FE results are shown below in Fig. S3. The surface profiles in these simulations do not show a region of constant mean curvature and are practically identical to the surface profiles obtained using the isotropic surface model.

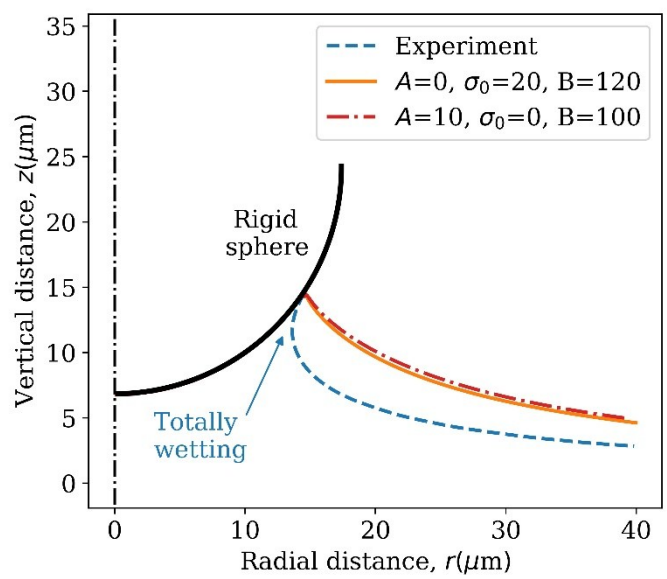

Fig. S3. Surface profiles for a 17.4-μm-radius sphere extracted from experimental data (blue dashed line) and finite element results (orange solid and red dash-dotted lines, respectively). The experimental surface profile indicates the totally wetting phenomenon near the contact line.

5 Comparison between neo-Hookean model and Yeoh model

To rule out the possibility that strain hardening of the gel may explain the discrepancy, we carry out one simulation using Yeoh model that allows for strain hardening. In simple tension test of our gel, specimens invariably break at the grips at a strain (engineering) close to or slightly above 100% (stretch ratio = 2) due to stress concentration as shown in Fig. S4 below.

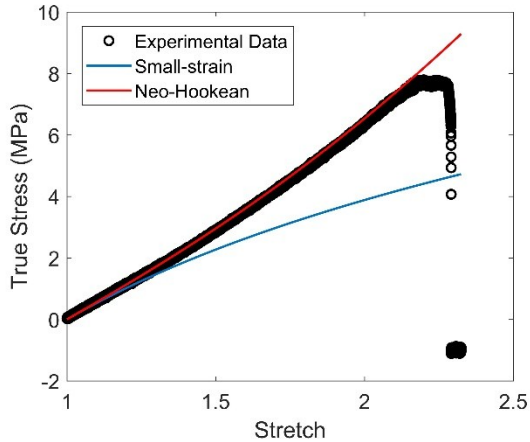

Figure S4. Comparison of the true stress–stretch behaviors of the small-strain and neo-Hookean models to experimental data in a uniaxial tension test. The black circles are the experimental data. The blue and red curves are the fittings of the small-strain elastic and neo-Hookean models, respectively. Note sample fails at a stretch ratio of approximately 2.3.

In Fig. S4 the neo-Hookean model fits the data very well for strains less than the failure strain (the fit uses the same small strain shear modulus μ in all our simulations). The material model in our simulation is based on equation (8) of the main text. The material parameters we used are: $C_1 = \mu / 2$, $C_2 / C_1 = -0.005$ and $C_2 / C_3 = 0.0001$. The *uniaxial* stress-strain curve for this set of parameters is shown in Fig. S4 as the dashed line. The prediction of the neo-Hookean model is also shown in the same figure as the solid line. In Fig. S5, P is the nominal stress and is normalized by the small strain shear modulus μ, and λ is the stretch ratio. Note that there is little difference between the two models for $\lambda \leq 2$.

The stresses for Yeoh solid near the contact line are plotted in Fig. S6 and corresponding results for the neo-Hookean solid are also plotted as a comparison. As expected, there is practically no difference between them. We also plot the surface profiles of both models in Fig. S7. Again, the difference is insignificant.

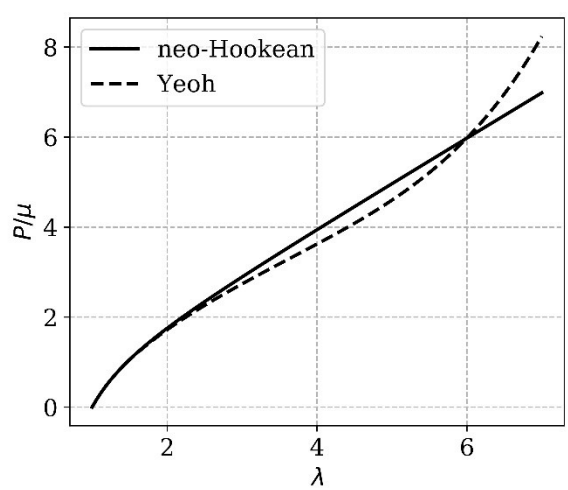

Fig. S5. Normalized nominal stress versus stretch for neo-Hookean and Yeoh materials, plotted as solid and dashed lines, respectively.

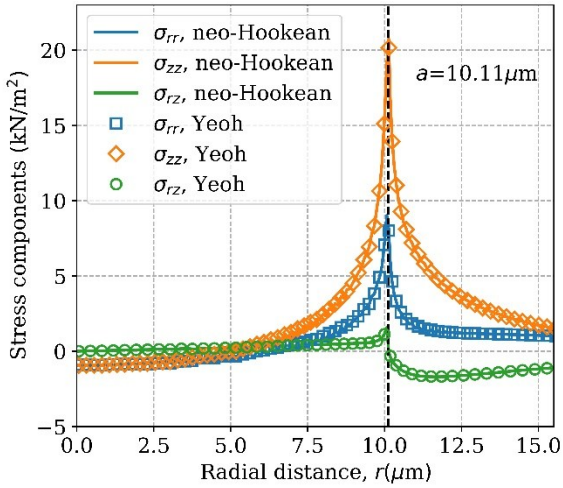

Fig. S6. Stress components of σ_{rr}, σ_{zz} and σ_{rz} for neo-Hookean and Yeoh models. The vertical black dashed lines indicate the contact radii at given imposed sphere displacements.

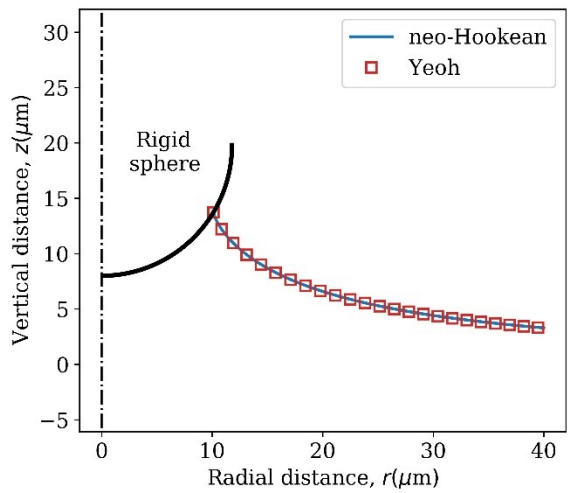

Fig. S7. Surface profiles of neo-Hookean and Yeoh models.

References

1 C.-Y. Hui, T. Liu, T. Salez, E. Raphael and A. Jagota, *Proceedings of the Royal Society A: Mathematical, Physical and Engineering Sciences*, 2015, **471**, 20140727–20140727.
2 K. E. Jensen, R. W. Style, Q. Xu and E. R. Dufresne, *Physical Review X*, 2017, **7**, 041031.
3 D. J. Steigmann and R. W. Ogden, *Proceedings of the Royal Society of London. Series A: Mathematical, Physical and Engineering Sciences*, 1999, **455**, 437.
4 M. E. Gurtin and A. Ian Murdoch, *Archive for Rational Mechanics and Analysis*, 1975, **57**, 291–323.
5 A. E. Green, P. M. Naghdi and W. L. Wainwright, *Archive for Rational Mechanics and Analysis*, 1965, **20**, 287–308.
6 M. P. do Carmo, *Differential geometry of curves and surfaces*, Prentice-Hall, Englewood Cliffs, N.J, 1976.
7 R. W. Style and Q. Xu, *Soft Matter*, 2018, **14**, 4569–4576.